OPTICAL ROUTER UTILIZING WAVEGUIDES COMBINED WITH BRAGG GRATINGS ON SILICON PHOTONIC

Dung Truong Cao, Hien Nguyen Trung, Duy Nguyen Thi Hang, Thuy Tran Thi Thanh
Posts and Telecommunications Institute of Technology

Abstract— This paper presents the operating principle of a 1×2 optical router and the numerical simulation design of its constituent components. The optical router comprises arrayed waveguide grating (AWG) structures, waveguide Bragg gratings (WGBG), a 1×2 optical switch utilizing 2×2 multimode interference (MMI) couplers, and wavelength-selective routing based on microring resonators for six high-density wavelength channels in dense wavelength-division multiplexing (DWDM) applications. Computational results from localized simulations for each component demonstrate excellent optical performance, validating the adherence to the design principles. These favorable outcomes indicate significant potential for the proposed structure in high-density wavelength-selective routing devices for DWDM optical communication systems and high-speed optical interconnects.

Keywords— optical router, arrayed waveguide grating (AWG), Bragg grating waveguide, microring resonator, numerical simulation, silicon photonics.

I. INTRODUCTION

Due to the explosive increase in the number of mobile terminal devices and the rapid development of multimedia applications and cloud computing services, the demand for transmission capacity and network bandwidth in optical networks has grown exponentially. Wavelength-division multiplexing (WDM) technology has emerged as the most widely used solution to meet the ever-increasing bandwidth requirements[1]–[3]. An essential device in WDM networks is the optical add-drop multiplexer (OADM). It can selectively remove/add one or more wavelength channels at a network node without the need for costly optical-electrical-optical (OEO) conversions.

In a WDM system, the waveguide routing is arranged in an Arrayed Waveguide Grating (AWG) array, acting as a key component. The AWG is specifically designed for channel multiplexing and demultiplexing, separating optical signals into individual wavelength channels. The AWG consists of an array of optical waveguides, which are typically planar structures that guide the optical signals. These waveguides are often designed to support a specific wavelength or range of wavelengths. WDM technology, with the help of AWGs, significantly increases the capacity of optical communication systems. By utilizing different wavelengths to carry distinct signals simultaneously, WDM allows for a higher data transmission capacity over a single optical fiber. Today, AWG (Arrayed Waveguide Grating) configurations offer flexibility in the management and upgrading of optical networks. Wavelength channels can be added or removed in a flexible manner. AWG also allows for high-density support of multiplexing and demultiplexing with channel spacing, for example, at intervals such as 0.2 nm, 0.4 nm, and 0.8 nm, in compliance with the ITU-T G.694.1 standard grid, ensuring high performance.

Additionally, in the planar waveguide technology, Bragg gratings have been utilized in various applications such as filters, dispersion compensation, pulse shaping [4], and more. Recently, the integration of Bragg grating waveguides on the silicon-on-insulator (SOI) platform has garnered increasing research interest. Narrow-band Bragg gratings prove highly useful in many applications, such as wavelength-division multiplexing (WDM) channel filters. To confine a narrow bandwidth, it is necessary to construct longer Bragg gratings with weak coupling. Bragg grating nano-waveguides exhibit strong mode confinement with disorder along the sidewalls, resulting in large coupling coefficients, even with bending amplitudes of only a few nanometers. To mitigate the coupling coefficient, spatially periodic refractive index disorder is placed away from the grating waveguide [5] or built on the sidewalls of the slab waveguide [6]. Since these are two-port devices, a 2 × 2 mode-selective coupler [7], asymmetric Y-branch [8], or adiabatic taper coupler [9] is required to eliminate Bragg reflection. However, achieving precise fabrication for such devices remains challenging.

A wavelength-routed optical router plays a crucial role in information systems based on Wavelength Division Multiplexing (WDM) technology, such as WDM fiber optic systems or high-speed optical interconnects in network-on-chip (NoC) optical systems. Some studied proposals of photonic integrated devices for optical wavelength router based on microring resonators allow to add/drop the optical wavelengths selectively, however, such structures require complex designs and need to be equipped with waveguide crossings elements [10]. Some configurations involve arrays of AWG matrices forming a sequence and permuting the order of wavelengths, resulting in inflexible configurations[11].

Contact author: Dung Truong Cao
Email: dungtc@ptit.edu.vn
Manuscript received: 11/2023, revised: 12/2023, accepted: 01/2024.

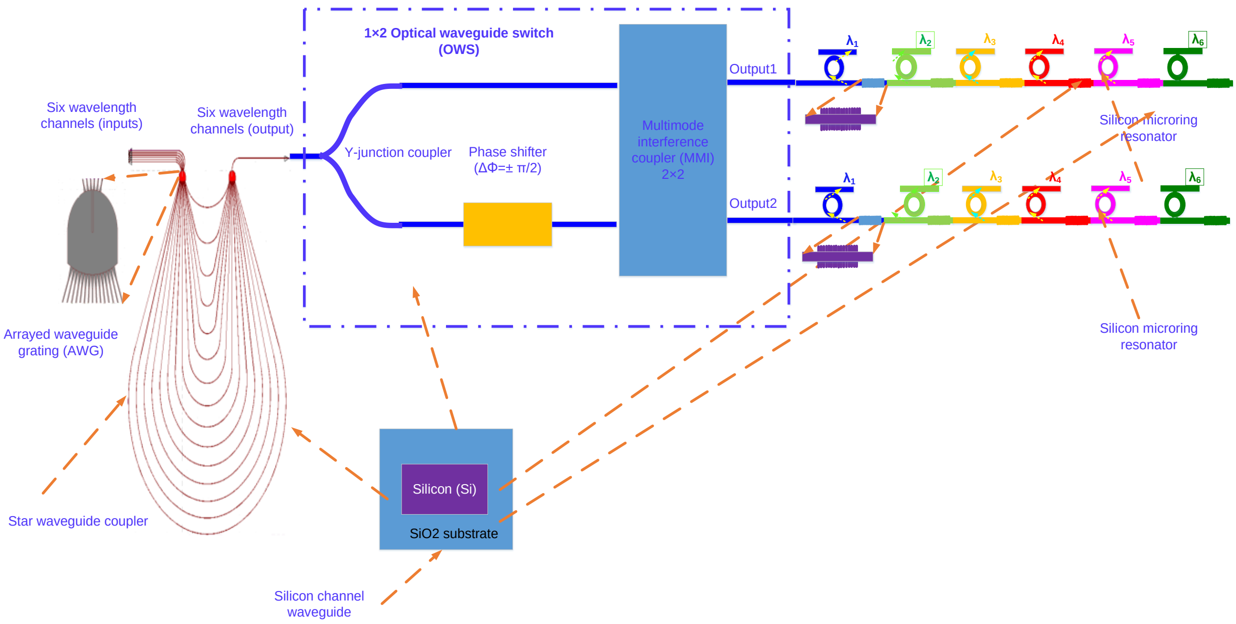

Figure.1. The principle design diagram of the optical router based on mode conversion and total internal reflection in silicon waveguides.

This paper presents a design study of a wavelength-routed optical router based on flat waveguide components on the Silicon-on-Insulator (SOI) platform compatible with CMOS fabrication processes. The design incorporates Arrayed Waveguide Gratings (AWG), Bragg scattering gratings, and is assisted by resonant ring couplers. The paper primarily focuses on the design principles of the AWG subsystem and the Bragg scattering gratings combined with microring resonators for wavelength-selective processing with six wavelengths following the standard ITU-T G.694.1 grid. The components were designed using the optical structure design tools BPM, GratingMode and FullwaveFDTD within the commercial software Rsoft.

II. STRUCTURAL DESCRIPTION AND ELEMENTAL DESIGN

Figure 1 illustrates the operational principle of an optical router for 6 channels conforming to the ITU-T G.694.1 grid with a channel spacing of 0.8nm and the first wavelength at 1549.32nm (corresponding to a frequency spacing of 100GHz and a central frequency of the first channel at 193.5THz). The structural system of the optical routing device consists of three main components, including a Wavelength Division Multiplexing (WDM) channel coupler using two Arrayed Waveguide Grating (AWG) structures for constructing a wavelength multiplexer, an Optical Waveguide Switch (OWS) switch, and a wavelength-selective demultiplexer based on Bragg scattering gratings combined with microring resonators. All elements in this investigation are designed for the transverse electric (TE) polarization state and based on channel waveguides fabricated from the standard silicon-on-insulator (SOI) wafer with the thickness of the silicon core layer of 220nm.

Initially, a system comprises 6 single-mode waveguides guiding 6 individual input wavelengths at 1549.32 nm, 1550.12 nm, 1550.92 nm, 1551.72 nm, 1552.52 nm, and 1553.32 nm with the wavelength spacing as much as 0.8nm corresponding to the frequency spacing of 100GHz, respectively. Subsequently, these 6 wavelengths pass through an AWG structured as an arrayed waveguide with 6 input ports and 15 output ports. Next, a star coupler connects these 15 waveguides to another AWG with 15 input ports and 1 output port. Thus, a system with two back-to-back configured AWGs creates a 6-channel wavelength multiplexer.

Next, a 1×2 switchable optical waveguide structure (OWS) consists of one input port and two output ports. The input port of this OWS structure initially passes through a symmetrical Y-junction coupler to split the incoming optical signal into two branches. Subsequently, two arms travel along two straight waveguides, with the lower branch passing through a phase shifter utilizing the thermo-optic effect generated by a thin metal film (Titanium metal) placed above a waveguide. Then, these two branches pass through a 2×2 multimode interference coupler (MMI) to combine the optical signals, creating the expected 1×2 switch mechanism. The 2×2 MMI interference coupler operates with 2 inputs and 2 outputs positioned at $\pm W_{MMI}/4$ (where W_{MMI} is the width of the MMI waveguide, and the coordinate axis is calculated along the vertical centerline of the MMI waveguide). The length of the MMI coupler is determined by:

$$L_{MMI} = 3L_{\pi} / 2 \quad (1)$$

where $L_\pi = \frac{4n_e W_e^2}{3\lambda}$ is the half-beat length of the MMI coupler, $W_e = W_{MMI} + \frac{\pi}{\lambda}\left(n_e^2 - n_c^2\right)^{-1/2}$ TE polarization mode.

Before connecting to the 2×2 MMI coupler, we place a controllable phase shifter with a suitable phase-shift to perform a mode demultiplexer's function by combing the optical fields from two access arms. The 2×2 MMI coupler in this design has the length $L_{MMI1} = 3L_\pi / 2$, leading to its transfer matrix is defined by [12]:

$$M_1 = \frac{1}{\sqrt{2}}\begin{pmatrix} 1 & j \\ j & 1 \end{pmatrix} \quad (2)$$

Hence, if the phase shifter has the phase difference $\Delta\Phi=\pm\pi/2$, the 2×2 MMI coupler will combine two optical paths from two arms of its input ports to the selectable outputs of the 2×2 MMI coupler.

Then, a waveguide Bragg grating (WGBG) based on a Bragg grating modulation scheme consists of a periodically modulated refractive index structure along the core of a single-mode optical waveguide. This modulation can either be in the form of a narrow-band modulation of the edge-relief type or a toothed comb-like modulation with an apodization profile in a uniform or cosine-shaped fashion. The entire waveguide structure is fabricated from a standard silicon-on-insulator (SOI) wafer, providing compatibility with Very Large-Scale Integration (VLSI) CMOS fabrication technology. When a broad-spectrum source is input, it produces a narrow-wavelength-reflected spectrum with resonant wavelengths known as Bragg wavelengths. The transmitted spectrum towards the output exhibits missing wavelengths corresponding to the Bragg wavelengths l_B. According to Bragg's law, the Bragg diffraction method based on dielectric or pure semiconductor waveguides (such as silicon, for example) will only reflect a specific wavelength known as the Bragg wavelength, determined by the formula [13]:

$$l_B = \frac{2n_{eff}\Lambda}{m} \quad (3)$$

Here, Λ is the Bragg wavelength, and n_{eff} is the effective refractive index of the waveguide core in optical diffraction, and m=1,2,3... represents the diffraction order, resonant order, or grating order. The operating principle of the waveguide Bragg diffraction is similar to that of fiber Bragg grating (FBG) diffraction.

The wavelength spacing between the first minima (refer to Figure 2), or bandwidth Δl, is determined by the refractive index modulation structure (as a transforming function) given by the equation:

$$\Delta l = \left[\frac{2\Delta nh}{p}\right] l_B \quad (4)$$

For the case of WGBG with width-modulated apodization or height-modulated apodization, the bandwidth Δl is determined according to the mode coupling theory by [14],[15]:

$$\Delta l = \frac{l_B^2}{p\, n_g}\sqrt{k^2 + (p/L)^2}\,, \quad k = \frac{\Gamma\left(n_1^2 - n_2^2\right)}{l_0 n_{eff}} \quad (5)$$

where l_B is the resonant reflection wavelength following the Bragg's law, n_g is the group velocity propagating into the grating, k is the coupling coefficient of the grating, L is the length of the grating. The strength of the coefficient k depends on the overlapping coefficient (also called as mismatched coefficient) Γ. For TE-polarized waves, solving the Maxwell's equations for guided waves in the waveguide Bragg grating yields a transcendental equation [14],[15] :

$$v\tan v = \left(\frac{V^2}{4} - v^2\right)^{1/2}, \text{ với } v = \frac{w}{2}\left(k_0^2 n_1^2 - b^2\right)^{1/2}, \quad (6)$$

where, $k_0 = \frac{2p}{l_0}$ is the wavenumber in vacuum (free space) with the operation wavelength l_0, the parameter V is determined by: $V = k_0 w\left(n_1^2 - n_2^2\right)^{1/2}$, w is the core width of the grating. Reflectivity R of the waveguide grating at the Bragg's resonant wavelength is determined by:

$$R = \frac{k^2 \sinh^2 gL}{g^2\cosh^2 gL + \frac{\Gamma^2}{4}\sinh^2 gL}, \text{ with } g^2 = k^2 + \frac{\Gamma^2}{4} \quad (7)$$

In which, the coupling coefficient k at the Bragg wavelength is followed as [16]:

$$k = k_B = \frac{2\left(n_1 - n_2\right)}{l_B} \quad (8)$$

Note that light diffraction of the grating occurs on a very small scale, typically l_B around 1 μm. Therefore, this property also makes diffraction highly beneficial in optical fiber communication systems.

Diffraction gratings are created in a comb-like pattern horizontally using electron beam lithography or extremely ultraviolet photolithography (EUV) with a periodic variation of δ_w = 1nm. The diffraction period is fixed at Λ = 0.005 μm with a sinusoidal grating profile. The grating is formed with a uniform apodized aperture. It can also be modulated by varying the core refractive index using germanium doping into the silicon core. However, in this study, we only consider the geometrically uniform diffraction structure. By designing diffraction structures with appropriate grating periods to achieve Bragg reflection at 6 selected wavelengths.

Finally, in a scenario of practical applications to filter the reflected wavelengths into separate channels in individual single-mode waveguides, we employ a resonant coupler combined with a diffraction structure to isolate each wavelength individually. According to the theory of resonant coupling, the mode matching between a straight waveguide and a loop (with radius r) having equal waveguide width (both in width and height within the waveguide structure) leads to the condition for resonant coupling when there is appropriate matching of the waveguide moments, given by [17]:

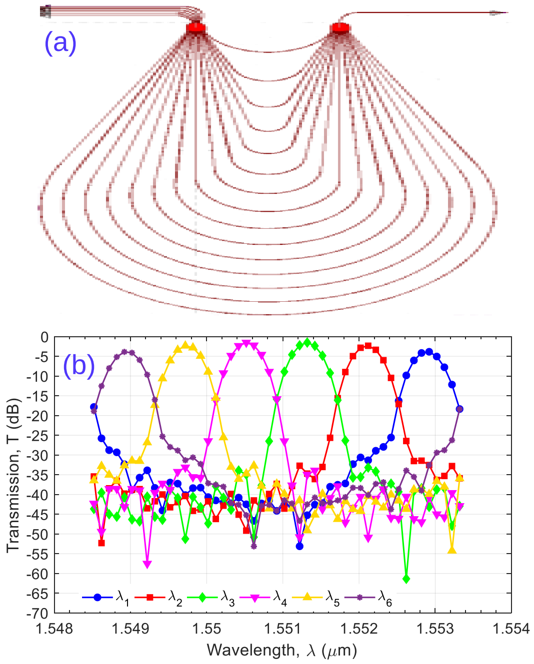

Figure.2. (a) Schematic design of AWGs with star couplers for creating a 6-channel DWDM multiplexer, (b) transmission response of the wavelength spectrum of the selected wavelength multiplexer.

$$m\lambda_m = 2\pi r n_{eff} \tag{9}$$

Here m is the mode number of the loop, λ_m corresponds to the resonant wavelength of the m^{th} mode, r is the radius of the loop, n_{eff} is the effective refractive index of the loop corresponding to the wavelength λ_m, and it depends on the waveguide width, the gap g, which is the coupling gap between the straight waveguide and the microring waveguide.

According to the theory of coupled-ring resonators, a coupled-ring resonator structure consists of a resonant ring, which is a ring-shaped waveguide (ring resonator) coupled with two straight waveguides oriented in parallel with separation gaps denoted as g_1 and g_2. The coupling coefficients due to the electric field interaction are denoted as k_1 and k_2, respectively. The loss coefficient of the ring resonator due to curved bend scattering and absorption is denoted as α, the insertion loss coefficient due to the straight waveguides is denoted as γ, and the radius of the coupled-ring resonator is denoted as r. In this case, the transfer function of the output (drop port) and input (input port) fields is determined by the equation [18]:

$$\frac{E_d}{E_i} = \frac{-\sqrt{k_1}\sqrt{k_1}Dc\exp(jf)}{1-\sqrt{1-k_1}\sqrt{1-k_1}c^2\exp^2(jf)} \tag{10}$$

where $D=(1-g)^{1/2}$, $c = D.\exp(-aL/4)$, $L = 2pr$, $f = 2Lpn_{eff}/l$, λ is the operation wavelength into the channel waveguides.

In symmetric design conditions, we set $g_1=g_2=g$, where the structures are identical in geometry and geometric symmetry. Consequently, $k_1=k_2=k$. The equations above aid in designing the coupled-ring resonator as a switch and help identify the optimal values for different parameters.

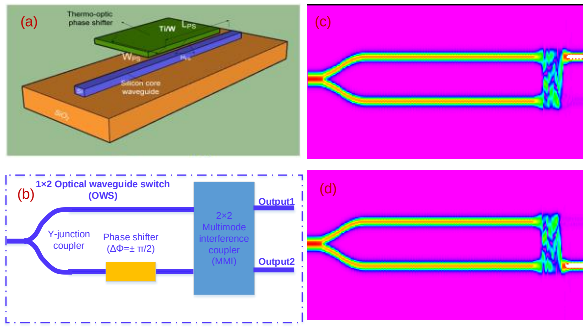

Figure.3. (a) structure diagram of the thermo-optic phase shifter (TOPS), (b) placement of TOPS in the 1×2 OWS structure, (c) 3D-BPM electric field pattern simulation for the phase shift $\Delta\Phi = \pi/2$, and (d) 3D-BPM electric field pattern simulation for the phase shift $\Delta\Phi = -\pi/2$.

By adjusting the radius of the microresonator, we resonate successively with each of the 6 selected wavelengths. This allows us to selectively route and drop each wavelength into dedicated single-mode waveguides. In this way, we conclude the process of path selection and add/drop functions of the designated wavelengths within the desired ITU grid.

III. NUMERICAL SIMULATION DESIGN OF ELEMENTS FOR THE PROPOSED ROUTER

Firstly, we design a six-channel multiplexer using AWGs based on channel waveguides with a silicon core and a silica glass (SiO_2) cladding. The refractive indices of the core and cladding are 3.465 and 1.45, respectively, at a wavelength of 1550nm. The width of the single-mode waveguide at the input and output is designed to guide independent wavelengths for the six selected wavelengths, and the output waveguide width for the combined spectrum of the six wavelengths is set to w=0.5μm (for single-mode guidance). To design the wavelength division multiplexer, we utilize the AWG Router tool in the commercial Rsoft software. This tool allows for the automatic design of the primary AWG waveguide structure using a reflective grating-type configuration with an initial converging lens structure at the input. Subsequently, the output ports are connected back-to-back to a secondary AWG structure with single-mode waveguides connected in a star coupler configuration. The output of the secondary AWG serves as a single output port for the spectrum of the 6 wavelengths. Figure 2(a) illustrates the CAD-assisted design of the structure, and Figure 2(b) shows the transmission characteristics of the combined spectrum of the 6 wavelengths. It is observed that the wavelength multiplexer enables high-density combining (channel spacing of about 100 GHz) with low crosstalk, as the noise signals are consistently lower than the peak signals of each wavelength by more than 30 dB. Next, we design an optical waveguide switch (OWS) structure in a 1×2 configuration. This structure consists of a single-mode input waveguide. A symmetrical Y-junction coupler, comprising sinusoidal waveguides, is used to split the optical path in a 50:50 ratio.

Subsequently, these two waveguides are straightened, and one arm is equipped with a phase shifter to control the switching. The phase shifter (PS) consists of a thin titanium film placed above the waveguide, acting as a resistive heater, separated from the waveguide by approximately 1 µm and powered by a direct current (DC) source in pulse form. Under the influence of a pulsed DC source, the Titanium metal thin film heats up and provides a localized hot spot beneath the waveguide. The heat source alters the refractive index of the silicon core in the thermal transition region, inducing an optical phase shift ΔΦ as a function of temperature. Subsequently, the two straight waveguides are connected to a 2×2 multimode interference coupler (MMI) at positions $\pm W_{MMI}/2$. This multimode coupler is designed with a length as $L_{MMI1} = 3L_\pi / 2$ to produce the corresponding phase matching in accordance with the transfer matrix in Equation (2). Therefore, if the phase shift ΔΦ=±π/2, the MMI coupler allows the combination of two optical paths into a selected optical signal at one of the two outputs, effectively creating a switching mechanism [12]. In this study, the width of the 2×2 MMI waveguide is chosen as W_{MMI}=3.8 µm, and the optimal length for the 2×2 MMI coupler to function as a perfect 3-dB coupler is determined to be $L_{MMI1} = 3L_\pi / 2$=56.8µm by using the 3D-BPM simulation tool in the Rsoft software. Figure 3(a) illustrates the structure of the Thermo-Optic Phase Shifter (TOPS), Figure 3(b) shows the placement of TOPS in the 1×2 OWS structure, and Figures 3(c, d) represent the simulation results obtained using the 3D-BPM method corresponding to phase shifts ΔΦ = π/2 and ΔΦ = -π/2, respectively.

Finally, a numerical simulation design for a wavelength filter based on the WGBG structure is proposed and simulated. Initially, the WGBG structure is considered as a channel waveguide structure. Gratings are created through a toothed comb pattern in the transverse direction using electron beam lithography or extremely ultraviolet (EUV) photolithography. The grating period is fixed at Λ =0.005 µm with sine-shaped grating profile. The grating structure is apodized uniformly. The grating can also be modulated by varying the refractive index of the core by incorporating germanium into the silica core. However, in this study, we only consider the grating structure that is geometrically apodized. This is compatible with the CMOS process for fabricating waveguides from standard SOI wafers (220nm Si core thickness on a 3µm SiO_2 glass BOX layer and a 2mm thick substrate)[19]. Using the GratingMode simulation tool from the Rsoft commercial software, we investigate the spectral characteristics and resonant wavelengths of the proposed structure. The simulation parameters are set to grating pitch ranging from 0.2µm to 0.5µm, modulation depth of apodization δ_w = 1nm, and rectangular or sine-shaped grating profiles with a duty cycle of 50%. The core width of the waveguide grating is w=0.5 µm with a Si core height of 220nm in the channel waveguide structure, supporting only the TE0 mode. The length of the WGBG waveguide is chosen to be relatively large, starting from 100µm. Next, we consider when the modulation depth of the grating teeth is δ_w=1nm and the desired Bragg reflection wavelength is 1550nm. Through GratingMod simulations, we investigate the full-width at half-maximum (FWHM) at the FWHM maximum point and the transmission efficiency at the corresponding peak wavelength of the Bragg resonance as a function of the length L of the grating. Figures 4(a, b) show that as the length of the grating increases, the FWHM generally decreases rapidly, and the transmission efficiency increases rapidly. When the grating length reaches a certain threshold value of about 2000µm=2mm, the FWHM and the peak transmission efficiency (nearly 100%) remain almost unchanged, indicating saturation. In this paper, to match with the integration of the proposed structure with resonant rings for filtering individual DWDM channels, the length of each filter for separating each wavelength is

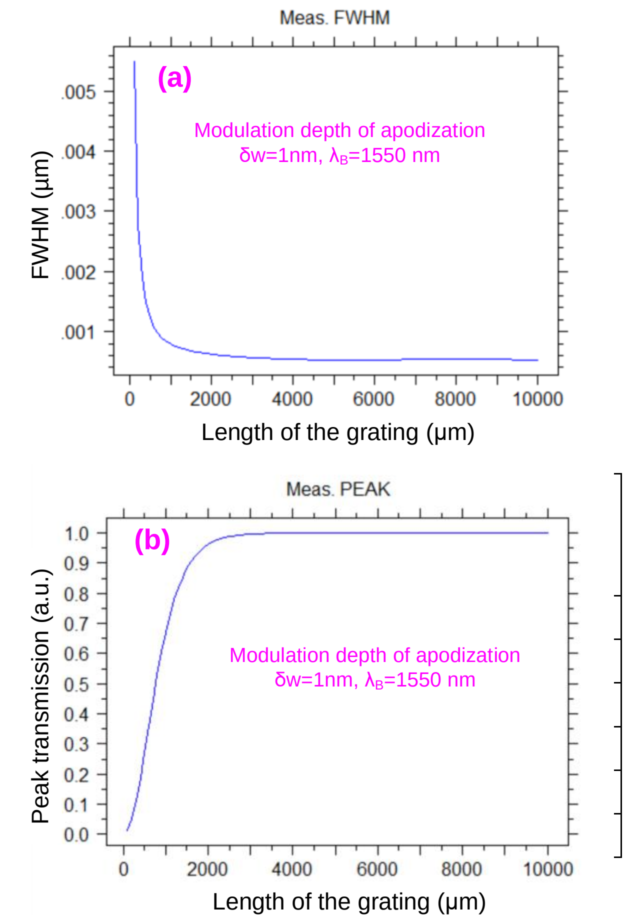

Figure 4. Simulation of the reflective spectral characteristics and Bragg resonance wavelengths at 1550nm with an apodization width of δw = 1nm and a grating width w=0.5µm as functions of the length of the grating for: (a) FWHM width and (b) peak transmission.

Table 1. Design parameters from numerical simulation by Grating tool for wavelength filter.

Central frequency (THz)	Central wavelength (nm)	Effective index	Grating period Λ (nm)
193	1553.32	2.6098	297.59
193.1	1552.52	2.6105	297.36
192.2	1551.72	2.6112	297.13
193.3	1550.92	2.6118	296.91
193.4	1550.12	2.6124	296.68
193.5	1549.32	2.6130	296.46

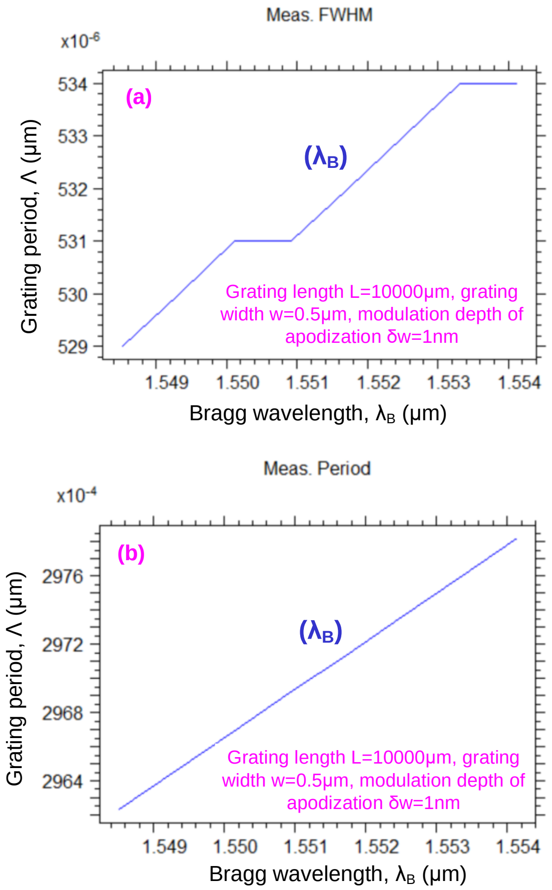

Figure 5. Simulation of reflective spectral FWHM characteristics and grating periods at the Bragg resonant wavelength of 1550nm with a length of L=10000µm, grating width w=0.5µm, and apodization width δ_w=1nm as a function of the wavelength response containing the necessary Bragg wavelengths designed for: (a) FWHM and (b) grating period Λ.

chosen as L=10000µm=10mm. Assuming that we want to find the grating period Λ for which, at that period, the resonant wavelength for Bragg reflection forms distinct wavelengths within the third telecom window at certain wavelengths according to the standard frequency grid and the central wavelength of the ITU-T.G694.1 recommendation with a channel spacing Δλ=0.8 nm, we use the GratingMod simulation tool to find the effective index and the corresponding grating period, as shown in the corresponding values presented in Table 1.

The spectral response of an optical device or a photonic device is crucial as it demonstrates the dynamic properties of the system. We investigate through numerical simulations using Coupled Mode Theory (CMT) for the grating dependent on the spectrum of the wavelengths studied in the C band of ITU-T.G694.1 and the channel spacing of 0.8 nm, along with some fixed design parameters such as L = 10000µm, w = 0.5µm, and δ_w = 1nm. Figure 5(a) shows that the FWHM increases linearly with the wavelength with a nearly linear ratio in the considered wavelength range in Table 1. We can see that the FWHM increases slightly, but in the DWDM wavelength range designed and used, it is still smaller than the channel spacing Δλ=0.8nm. Similarly, Figure 5(b) shows that the grating period increases proportionally with the Bragg wavelength requiring reflection. This is because we design a first-order diffraction structure in the grating, and within the C band, with a relatively wide waveguide width w=0.5µm, the broad spectral response with an effective refractive index (neff) maintaining a nearly constant value over the range from 1525nm to 1625nm (containing the C+L band of the third telecom window) is obtained. Therefore, using Equation (3) with $l_B = \frac{2n_{eff}\Lambda}{m}$, we will obtain the linear characteristics of Λ as a function of the wavelength response, as presented in Table.1.

Finally, by utilizing FDTD simulations to design suitable microring resonators, we sequentially branch the wavelengths (among the chosen six wavelengths), where each wavelength is coupled with a microring resonator. In this design, all microring resonators are configured with a waveguide width of w=500nm and a gap size of g=150nm. We vary the radius r in the range of 3 to 4 µm to find the resonant wavelength at λ=1550.92nm, with the optimized radius found through FDTD simulation being r = 3.74µm, as illustrated in Figure 6. Similarly, by adjusting the values of the radius differently, we successively find suitable radii for resonating with the other listed wavelengths, as presented in Table 1, to entirely separate each remaining wavelength. The values obtained through FDTD simulations for the microring resonators are summarized in Table 2. The results indicate attenuation levels due to the microring resonators within the range of approximately 0.52dB to 0.65dB, corresponding to efficiencies ranging from a minimum of 86% (attenuation of 0.65dB) to around 89%. These results demonstrate practical applicability in the design and fabrication of optical wavelength multiplexers for routing individual wavelengths within the ITU-T G964.1 grid. Thus, the filtering of DWDM wavelengths using a Bragg grating waveguide structure combined with microring resonators has been successfully achieved. The results of this investigation are useful and comparable to the proposed structure that was published by Wu et al. [20] before.

IV. CONCLUSION

This article has elucidated the operational principles of a 1×2 optical router designed for six wavelength channels, utilizing AWG structures, Bragg gratings, MMI couplers, and microring resonators to filter DWDM wavelengths. The resulting optical routers efficiently distribute signals across six high-density channels, each with a channel spacing of Δλ=0.8nm, aligning with the recommendations of ITU-T.G.694.1. Numerical simulations of the optimized individual components have illustrated their local performance satisfaction. Furthermore, the proposed structure is adaptable for manipulation, allowing for the extension to multi-port routers accommodating numerous higher-density DWDM channels with smaller channel spacing, like Δλ=0.4nm, making it well-suited for high-capacity optical DWDM communication systems.

ACKNOWLEDGEMENT

This research is funded by Posts and Telecommunication Institute of Technology under the grant number 07-HV-2023-ĐT1.

REFERENCES

[1] G. C. Mandal and A. S. Patra, "High capacity hybrid WDM/TDM-PON employing fiber-to-the-home for triple-play services with 128 ONUs," *J. Opt.*, vol. 46, no. 3, pp. 347–351, 2017, doi: 10.1007/s12596-017-0410-5.

[2] S. Ullah *et al.*, "Optical Multi-Wavelength Source for Single Feeder Fiber Using Suppressed Carrier in High Capacity LR-WDM-PON," *IEEE Access*, vol. 6, pp. 70674–70684, 2018, doi: 10.1109/ACCESS.2018.2880426.

[3] F. Donati Simões, D. Moutinho Pataca, and M. Lacerda Rocha, "Design of a comb generator for high capacity coherent-WDM systems," *IEEE Lat. Am. Trans.*, vol. 10, no. 3, pp. 1690–1696, 2012, doi: 10.1109/TLA.2012.6222572.

[4] J. Chen, B. Liu, and H. Zhang, "Review of fiber Bragg grating sensor technology," *Front. Optoelectron. China*, vol. 4, no. 2, pp. 204–212, 2011, doi: 10.1007/s12200-011-0130-4.

[5] H. Y. D. Yang and D. R. Jackson, "Theory of line-source radiation from a metal-strip grating dielectric-slab structure," *IEEE Trans. Antennas Propag.*, vol. 48, no. 4, pp. 556–564, 2000, doi: 10.1109/8.843669.

[6] C. S. Huang and W. C. Wang, "SU8 inverted-rib waveguide Bragg grating filter," *Appl. Opt.*, vol. 52, no. 22, pp. 5545–5551, 2013, doi: 10.1364/AO.52.005545.

[7] A. Maese-Novo *et al.*, "Wavelength independent multimode interference coupler," *Opt. Express*, vol. 21, no. 6, p. 7033, 2013, doi: 10.1364/oe.21.007033.

[8] W. Chang *et al.*, "An Ultracompact Multimode Waveguide Crossing Based on Subwavelength Asymmetric Y-Junction," *IEEE Photonics J.*, vol. 10, no. 4, pp. 1–8, 2018, doi: 10.1109/JPHOT.2018.2847762.

[9] L. Xu *et al.*, "Compact high-performance adiabatic 3-dB coupler enabled by subwavelength grating slot in the silicon-on-insulator platform," *Opt. Express*, vol. 26, no. 23, p. 29873, 2018, doi: 10.1364/oe.26.029873.

[10] J. Zhang, N. Wu, F. Ge, F. Zhou, and W. Xu, "Design of WDM-Based Optical Networks-on-Chip Router for Low Insertion Loss and Crosstalk," in *2021 IEEE 4th International Conference on Electronics Technology, ICET 2021*, 2021, pp. 1068–1072. doi: 10.1109/ICET51757.2021.9451093.

[11] P. T. Wu, W. N. Shih, and T. C. Liang, "Design of optical router with bidirectional interleaver and OXC functions," in *Proceedings of 4th IEEE International Conference on Applied System Innovation 2018, ICASI 2018*, 2018, pp. 1159–1162. doi: 10.1109/ICASI.2018.8394490.

[12] H. Ta Duy *et al.*, "1×2 switchable dual-mode optical 90° hybrid device based on thermo-optic phase shifters and 2×2 MMI couplers on SOI platform," *IEEE Photonics J.*, pp. 1–1, 2021, doi: 10.1109/jphot.2021.3055691.

[13] C. Alonso-Ramos *et al.*, "Diffraction-less propagation beyond the sub-wavelength regime: a new type of nanophotonic waveguide," *Scientific Reports*, vol. 9, no. 1. 2019. doi: 10.1038/s41598-019-41810-0.

[14] H. A. Haus and R. V. Schmidt, "Approximate analysis of optical waveguide grating coupling coefficients," *Appl. Opt.*, vol. 15, no. 3, p. 774, 1976, doi: 10.1364/ao.15.000774.

[15] Y.-J. Hung *et al.*, "Narrowband silicon waveguide Bragg reflector achieved by highly ordered graphene oxide gratings," *Opt. Lett.*, vol. 42, no. 22, p. 4768, 2017, doi: 10.1364/ol.42.004768.

[16] W. Zhang and J. Yao, "A fully reconfigurable waveguide Bragg grating for programmable photonic signal processing," *Nat. Commun.*, vol. 9, no. 1, pp. 1–9, 2018, doi: 10.1038/s41467-018-03738-3.

[17] D. . Rabus, "Ring Resonators: Theory and Modeling, in Integrated Ring Resonators," in *Integrated Ring Resonators*, Springer, 2007, pp. 3–40. [Online]. Available: http://www.springer.com/978-3-540-68786-3d

[18] J. K. Rakshit, T. Chattopadhyay, and J. N. Roy, "Design of ring resonator based all optical switch for logicand arithmetic operations - A theoretical study," *Optik (Stuttg).*, vol. 124, no. 23, pp. 6048–6057, 2013, doi: 10.1016/j.ijleo.2013.04.075.

[19] F. Xia, M. Rooks, L. Sekaric, and Y. Vlasov, "Ultra-compact high order ring resonator filters using submicron silicon photonic wires for on-chip optical interconnects," *Opt. Express*, vol. 15, no. 19, p. 11934, 2007, doi: 10.1364/oe.15.011934.

[20] P. T. Wu and T. C. Liang, "Design of novel fiber optical flexible routing system," *Applied Sciences (Switzerland)*, vol. 9, no. 22. 2019. doi: 10.3390/app9224763.

BỘ CHỌN ĐƯỜNG QUANG SỬ DỤNG ỐNG DẪN SÓNG KẾT HỢP VỚI CÁCH TỬ BRAGG TRÊN PHOTONIC SILICON

***Tóm tắt*—** Bài báo này trình bày nguyên lý hoạt động của bộ chọn đường quang 1×2 và thiết kế mô phỏng số các thành phần cấu thành của nó. Bộ chọn đường quang bao gồm các cấu trúc cách tử ống dẫn sóng phân mảng (AWG), cách tử Bragg ống dẫn sóng (WGBG), một công tắc quang 1×2 sử dụng bộ ghép giao thoa đa mode 2×2 (MMI) và chọn đường chọn lọc bước sóng dựa trên bộ cộng hưởng vòng vi mô cho sáu bộ cộng hưởng vòng mật độ cao. các kênh bước sóng trong các ứng dụng ghép kênh phân chia bước sóng (DWDM) dày đặc. Kết quả tính toán từ các mô phỏng cục bộ cho từng thành phần cho thấy hiệu suất quang học vượt trội, xác nhận việc tuân thủ các nguyên tắc thiết kế. Những kết quả thuận lợi này cho thấy tiềm năng đáng kể của cấu trúc được đề xuất trong các thiết bị chọn đường chọn lọc bước sóng mật độ cao cho hệ thống thông tin quang DWDM và các kết nối quang tốc độ cao.

Từ khóa— bộ định tuyến quang, cách tử ống dẫn sóng phân mảng (AWG), ống dẫn sóng cách tử Bragg, bộ cộng hưởng vòng micro, mô phỏng số, quang tử silicon.

Dung Truong Cao was born in Thanh Hoa, Vietnam, in 1980. He received the Engineer, Master of Science, and Ph.D. degrees from Hanoi University of Science and Technology, Hanoi, in 2003, 2006, and 2015, respectively. He is currently a Lecturer in the Department of Electronic Engineering1, Posts and Telecommunications Institute of Technology, Hanoi, Vietnam. His research interests include photonic integrated circuits, plasmonics, high-speed optical communication systems, smart IoT networks, applications

of deep learning models for photonics design, and AI in photonics. Email: dungtc@ptit.edu.vn

Hien Nguyen Trung was born in 1973. He graduated in 1995 from the Hanoi University of Science and Technology with an engineer degree in Electronics and Informatics Engineering. He obtained a Master degree in Electronics and Telecommunications from the Posts and Telecommunications Institute of Technology (PTIT) in 2008. Currently, he is pursuing the doctoral program about computer engineering discipline. His research interests include digital transmission, IP network performance, next-generation networks, terrestrial digital television, and neural networks. You can contact him via email at nthien.tu@bacninh.gov.vn.

Duy Nguyen Thi Hang was born in Quang Ninh province, Vietnam, in 1997. She received the Engineer, and Master of Science degrees at the Posts and Telecommunications Institute of Technology, Hanoi, in 2020, 20023, respectively. She is currently a Lecturer in the Department of Telecommunication Engineering1, Posts and Telecommunications Institute of Technology, Hanoi, Vietnam. She is now pursuing the doctoral program of data engineering at the Gunma University, Japan. Her research interests include photonic integrated circuits, optical communication systems, applications of AI models for big data processing and analyzing. Email: duynth@ptit.edu.vn

Thuy Tran Thi Thanh graduated from the Posts and Telecommunications Institute of Technology, earning both a Bachelor's and Master's degree in Telecommunications Engineering in 2021 and 2023, respectively. Currently, she serves as a lecturer in the Department of Electronic Engineering at the Posts and Telecommunications Institute of Technology. Additionally, she is pursuing a Ph.D. in Electronic Engineering. Her primary research interests encompass integrated optoelectronic circuits, high-speed optical communication systems, IoT-connected sensor networks, the application of artificial intelligence in signal quality processing, and the use of deep learning in inverse design problems. Email: thuyttt@ptit.edu.vn.